V European Conference on Computational Fluid Dynamics
ECCOMAS CFD 2010
J. C. F. Pereira and A. Sequeira (Eds)
Lisbon, Portugal,14-17 June 2010

THE IMPACT OF CYLINDER ROUGHNESS ON THE DRAG FORCES AND HEAT TRANSFER

F. Dierich and P. A. Nikrityuk

CIC Virtuhcon, Technische Universität Bergakademie Freiberg,
Fuchsmühlenweg 9, 09596 Freiberg, Germany
e-mail: frank.dierich@vtc.tu-freiberg.de
e-mail: petr.nikrityuk@vtc.tu-freiberg.de

Key words: convective heat transfer, roughness, immersed boundary method

Abstract. *This work presents a numerical investigation of the influence of the roughness of a cylindrical particle on the drag coefficient and the Nusselt number at Reynolds numbers (Re) up to 200, where the flow at the* $Re > 46$ *was unsteady. The heated cylindrical particle is placed horizontally in a uniform flow. Immersed Boundary Method (IBM) with a continuous forcing on a fixed Cartesian grid is used. The governing equations are the Navier–Stokes equation and the conservation of energy. A finite-volume based discretization and the SIMPLE algorithm with collocated-variables and Rie-Chow stabilization were used to solve the set of equations. Numerical simulations showed that the impact of the roughness on the drag coefficient is neglegible in comparison to the the surface averaged Nusselt number. In particular, the Nusselt number decreases rapidly with increase of the roughness thickness. The comparative analysis of results showed that the dependency of the efficiency factor* E_f *on the the surface enlargement coefficient* S_{ef} *can be approximated by the following relation* $E_f \approx S_{ef}^{-\frac{5}{4}}$ *for* $10 \leq Re \leq 200$.

1 Introduction

Flow past a circular cylinder is a well accepted *'benchmark'* tool to study the drag forces and heat transfer in bluff body wakes, e.g. see [1]. The extensive review of numerical investigations of the flow dynamics past a cylinder (done in early 1980s) can be found in [3]. It is a well known fact that at Reynolds numbers, $1 < Re < 46$, the flow past a cylinder is laminar, where a steady recirculation region with toroidal vortex occurs behind the cylinder. The size of the recirculation region grows with increasing Reynolds number. Here the Reynolds number is defined as $Re = 2R\,U_0/\nu$, where R is the radius of cylinder, U_0 is the free-stream velocity, and ν is the kinematic viscosity. At Reynolds numbers $Re \geq 46$, the flow becomes unsteady with vortex shedding (von Karman vortex shedding) in the near wake behind the cylinder. Many simulations were done to study the role of convection on the heat transfer near the cylinder, e.g. see [5], including the influence of a porous layer around the cylinder on the enhancement of the heat transfer, see the work done by [6]. In particular, Bhattacharyya & Singh [6] showed that a thin porous wrapper, which has the same thermal conductivity as the cylinder, can significantly reduce the heat transfer. To model the gas flow inside the porous layer they used the Dupuit-Forchheimer relationship, which states that the velocity inside the porous media is proportional to the bulk velocity multiplied by the porosity. The use of this assumption or the Darcy low assumption for the modeling of particle roughness is questionable due to the fact that the convection may not be negligible within the roughness region. The present work investigates the flow and heat transfer from a rough solid cylinder placed horizontally in a cross-flow with an uniform stream of air which has the Prandtl number of 0.5. The cylinder is assumed to be heated with a uniform surface temperature. The temperature difference between the free stream flow and the surface of the cylinder is equal to 20 K.

We consider the roughness layer to be made from the same material as the cylinder. Thus, the main motivation of this study is to estimate the influence of the thickness of roughness layer on the heat transfer and on the drag coefficient for a cylindrical particle. The practical context of this study is to take into account the particle roughness by the modeling of fluidized beds.

2 Problem formulation and governing equations

By neglecting the viscous heating effect and assuming constant thermophysical properties the incompressible Navier-Stokes equations and the energy equation in the temperature formulation have the following form:

$$\nabla \cdot \vec{u} = 0, \tag{1}$$

$$\frac{\partial \vec{u}}{\partial t} + (\vec{u} \cdot \nabla)\,\vec{u} = -\frac{\nabla p}{\rho} + \nu \nabla^2 \vec{u} - \nu \frac{\vec{u}}{K}, \tag{2}$$

$$\frac{\partial T}{\partial t} + (\vec{u} \cdot \nabla)\,T = \frac{\lambda}{\rho c_p} \nabla^2 T - \frac{1}{\rho c_p} \frac{(T - T_s)}{K}. \tag{3}$$

Here $\vec{u}$ is the velocity vector, p is the pressure, ν is the kinematic viscosity, λ is the thermal conductivity, ρ is the density, c_p is the heat capacity, T_s is the temperature of the particle. To set the boundary conditions on the particle surface we treat the interface as porous with a permeability coefficient given by:

$$K = \frac{\epsilon^3}{c_1 \left(1-\epsilon\right)^2}, \qquad c_1 = 10^5 \, \Delta x_{max}^{-1} \tag{4}$$

where $\epsilon \in [0,1]$ is the volume fraction of gas and Δx_{max} is the edge length of the largest control volume. To calculate the volume fraction of gas in each control volume we use a two-step algorithm. The first step in this algorithm is the description of the particle shape by a polygon. The second step uses the Sutherland-Hodgman clipping algorithm, for details see [7], to calculate the volume fraction of solid based on a polygon intersection with the 'walls' of a control volume. No-slip boundary conditions were set up on the cylinder surface by use of the source term $\frac{\vec{u}}{K}$ in eq.(2), for details see the work [14]. It should be noted here, that the source terms in eqs.(2) and (3) are activated automatically, see eq.(4), only in the cells occupied by the solid and interface corresponding to the case if $\epsilon \neq 1$. The thickness of the 'porous' interface equals to one control volume cell, where $\epsilon \neq 0$ and $\epsilon \neq 1$.

The principal scheme of the domain is shown in Fig. 1. The rough particle consists of an outer cylinder with the radius R and $n = 10$ notches with the depth $d \cdot R$ as shown in Figure 1. The size of the domain is shown in Fig. 1. The cylindrical particle is placed in the center of the domain with a total length of $L_1 = 140\,R$ and a total width of $L_2 = 80\,R$, where the center of the cylinder is placed in the point $(0,0)$. The depth of the notches $d \cdot R$ is varied from 0 to $0.5\,R$ by changing the parameter d from 0 to 0.5 to simulate different roughness.

3 Numerics and Validation

The set of transport equations has been discretized by a finite-volume, finite-difference based method. The SIMPLE algorithm with collocated-variables arrangement was used to calculate the pressure and the velocities, for details see [9]. Rhie and Chow stabilization scheme was used for the stabilization of pressure-velocity coupling, see [10].

To set up the 'internal' boundary conditions on the particle surface the source terms $-\nu\frac{\vec{u}}{K}$ and $-\frac{1}{\rho c_p}\frac{(T-T_s)}{K}$ in eqs.(2) and (3), respectively, are linearized following recommendations given by [8] as follows:

$$S = S_C + S_P \phi_P^{bc} \tag{5}$$

where ϕ_P^{bc} is the value of principal variable (T_s or u_s) inside the solid region. Applied this equation in our case we have:

$$S_C^u = 0, \;\; S_P^u = -\nu\frac{1}{K} \qquad S_C^T = \frac{1}{\rho c_p}\frac{T_s}{K}, \;\; S_P^T = -\frac{1}{\rho c_p}\frac{1}{K} \tag{6}$$

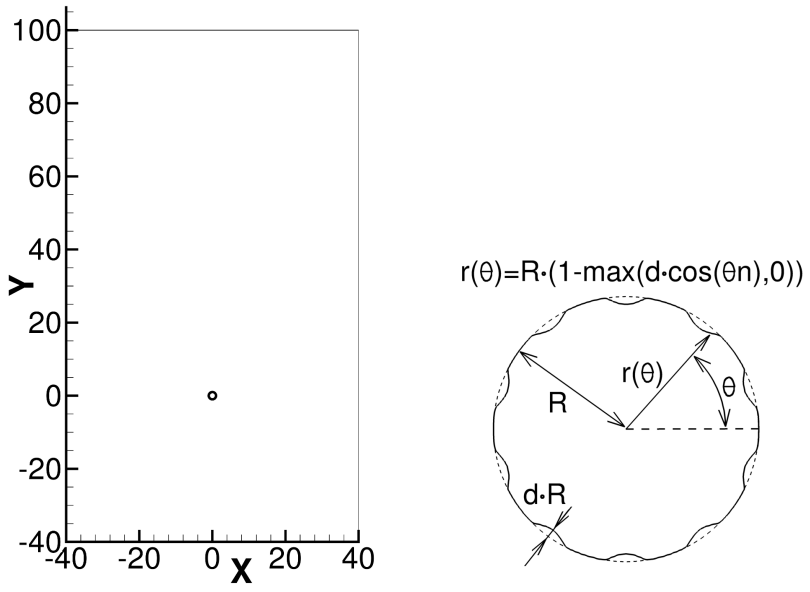

Figure 1: Size of the domain (links) and zoomed view of the particle (right) under investigation with roughness parameter d.

Here the term $\frac{1}{K}$ is nothing else than a number large enough to make the other terms in the discretization equation negligible in such a way that:

$$S_C + S_P T_P \approx 0, \qquad T_p = -\frac{S_C^T}{S_P^T} = T_s \tag{7}$$

Time marching with fixed time step was used. For every time step the outer iterations were stopped if the normalized maximal residual of all equations is less than 10^{-10} corresponding to 10 orders of magnitude. We used a grid with 400×600 control volumes. The size of a control volume (CV) inside the solid particle is about one hundredth of the particle diameter. This is achieved by local refinement of the grid inside the particle. The time step was equal to 0.1 sec, which is in non–dimensional time $6.25 \cdot 10^{-4}$. To validate the code and the model we reproduced the results of the flow around a cylinder at Reynolds number $Re = 20$. We compared the drag coefficient C_D, the angel of separation θ_s and the vortex length L/R, where R is the radius of the cylinder as shown in Figure 2. Table 1 shows that the present results are in good consistent with other data published.

Next, we validated our model and the code against experimental results of [11, 12]. The test case compares the numerical prediction of temperature profiles along the symmetry lines with experimental data. The experimental set up included a heated inner cylinder placed in the center of another cold cylinder. Due to the gravity field a buoyancy-induced flow occurs. The temperature contour plot and the flow pattern are shown in Fig. 3. The comparison of temperature profiles along the symmetry line compared with the data of [11, 12] are given in Fig. 4. It can be seen that the agreement between our predictions

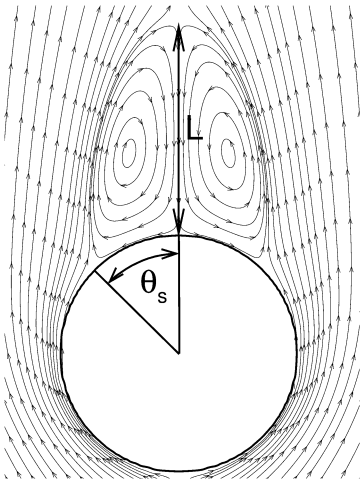

Figure 2: Definition of angel of separation (θ_s) and the vortex length (L)

Authors	C_D	θ_s	L/R
[5]	1.99	43.24	1.79
[2]	2.000	45.3	1.82
[4]	2.152	42.96	1.842
Present	1.99	43.9	1.86

Table 1: Validation I: fluid flow past a cylinder. The definition of parameters θ_s and L/R is given in Fig. 2.

and the experimental data is very good.

4 Results

To proceed with the analysis of results we describe shortly the main input parameters we use to study the system behavior shown in Fig. 1. The inflow velocity is calculated from the Reynolds number given by:

$$Re = \frac{u_{in}\, 2\, R}{\nu} \tag{8}$$

where R is the outer cylinder radius, see Fig. 1. To study the heat transfer characteristics we use the Nusselt number. In particular, we introduce the surface–averaged Nusselt number Nu_{av} given as follows:

$$Nu_{av} = \frac{\oint_S Nu_{local}\, ds}{\oint_S 1\, ds}, \qquad Nu_{local} = \frac{2\, R}{T_s - T_\infty} \frac{\partial T}{\partial n} \tag{9}$$

where Nu_{local} is the local Nusselt number, T_∞ is the free stream temperature, T_s is the particle surface temperature and n is the inward-pointing normal.

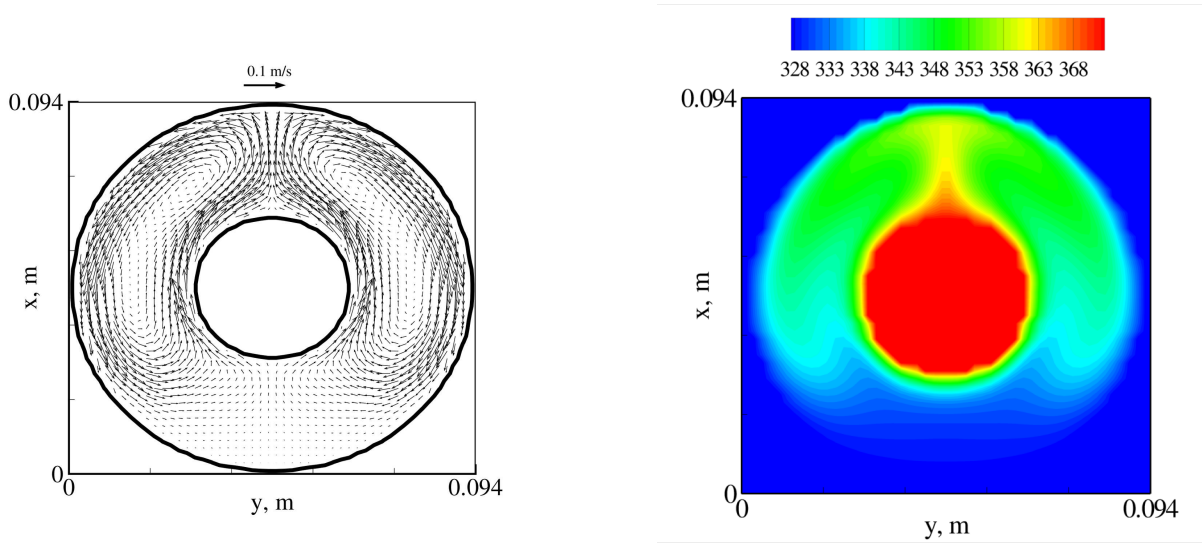

Figure 3: Validation II: The spatial distribution of the velocity vectors (left) and contour plot of the temperature (right). Here the temperature is given in Kelvin.

In order to study the influence of roughness on the heat transfer we introduce the heat transfer efficiency factor E_f, [6], given by:

$$E_f = \frac{Nu_{av}}{Nu_{av}^0} \tag{10}$$

where Nu_{av}^0 is the surface average Nusselt number for the particle with zero roughness. Thus, E_f measures the ratio between the average rate of heat transfer from a rough particle to the average rate of heat transfer from a particle without roughness. Thus, $E_f > 1$ corresponds to heat transfer enhancement and $E_f < 1$ corresponds to insulation.

The last parameter to characterize the roughness is the surface enlargement S_{ef} given by:

$$S_{ef} = \frac{S_{rough}}{S_0} \tag{11}$$

where S_0 and S_{rough} are the geometric surface area of the particle without roughness and with roughness, respectively.

The equation for the calculation of the drag coefficient have the following form:

$$C_D = \frac{F_D}{\rho u_\infty^2 R} \qquad \vec{F} = \oint \left(-p\vec{n} + \nu\left(\nabla\vec{u} + \nabla\vec{u}^T\right)\cdot\vec{n}\right) ds \tag{12}$$

In this work the numerical simulations were done for five Reynolds numbers 10, 20, 40, 100 and 200. For each Reynolds number we investigate systematically the influence of the roughness of the cylinder on the surface averaged Nusselt number. The roughness of the particle is varied through the increase of d, see Fig. 1.

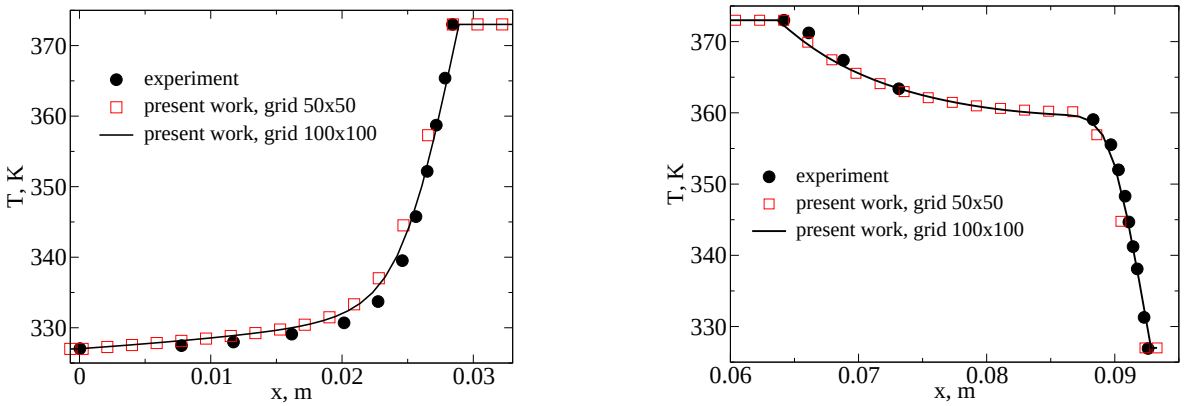

Figure 4: Validation II: The temperature profiles at the vertical symmetry line. Here the experimental data correspond to the results of [11, 12]

S_{ef}	d	Re = 10	Re = 20	Re = 40
1.00	0.00	2.76	1.99	1.50
1.08	0.10	2.74	1.98	1.49
1.29	0.20	2.76	2.00	1.50
2.12	0.50	2.93	2.12	1.60

Table 2: Drag coefficient (C_D) in different Re and S_{ef}

Fig. 5 shows an example of the velocity distribution near the particle surface for Re = 40 and $d = 0.50$. It can be seen that the velocity is zero in the dimples. Thus, the air in the dimples plays the role of an isolator, which decreases the convective heat transfer. This effect can be clearly seen in the Fig. 6, which depicts the contour plots of the nondimensional temperature $\frac{T-T_\infty}{T_s-T_\infty}$ for different Re and roughness ratios. It should be noted that in the case of $Re = 100$ we used time-averaging procedure to obtain the spatial distribution of the mean time temperature. Fig. 7 shows the snapshot of the nondimensional temperature contour plot calculated for $Re = 100$. Our results show that due to the 'isolation' effect produced by the dimples the thermal boundary layer thickness increases in comparison to the cases with less roughness. Thus, the temperature gradient in the dimples is decreased. But at the same time we have the increase of the temperature gradient in front of the stagnation point on the particle surface. This can be seen in the Fig. 8, which shows contour plots of the non-dimensional temperature gradient $\sqrt{\frac{\partial T}{\partial x}^2 + \frac{\partial T}{\partial y}^2}\frac{2R}{\Delta T}$. It can be seen that the local heat transfer changes dramatically. In particular, we have temperature gradients concentrated on the particle ledges. This effect can play a very import role at the combustion of rough particles leading to the local speed-up of combustion rate on the convex shaped interfaces.

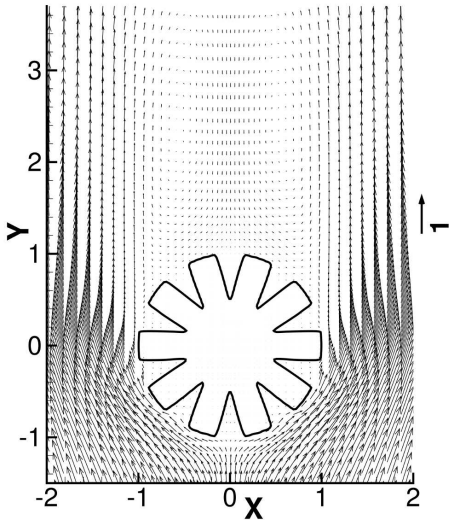

Figure 5: Velocity plot of non-dimensional vectors $\frac{\vec{u}}{u_{in}}$ in Re = 40 and $d = 0.5$, $S_{ef} = 2.12$

Next, we show the contour plots of the non-dimensional temperature, see Fig. 6. The increase of the Re number at a constant value of S_{ef} leads to the decrease of the thermal boundary layer, which is well know fact. But at the same time the increase of the surface enlargement at a constant value of Re leads to the increase of the thickness of the effective thermal boundary layer and as a result, the surface averaged Nusselt number decreases with the increase of S_{ef}. This effect is demonstrated in Fig. 9. It can be seen that the efficiency factor E_f is proportional to the surface enlargement coefficient S_{ef} as follows $E_f = S_{ef}^{-\frac{5}{4}}$.

In comparison to the behavior of the Nusselt number, the drag coefficient C_D increases insignificantly, up to 7%, with the increase of the roughness, see Tab. 4.

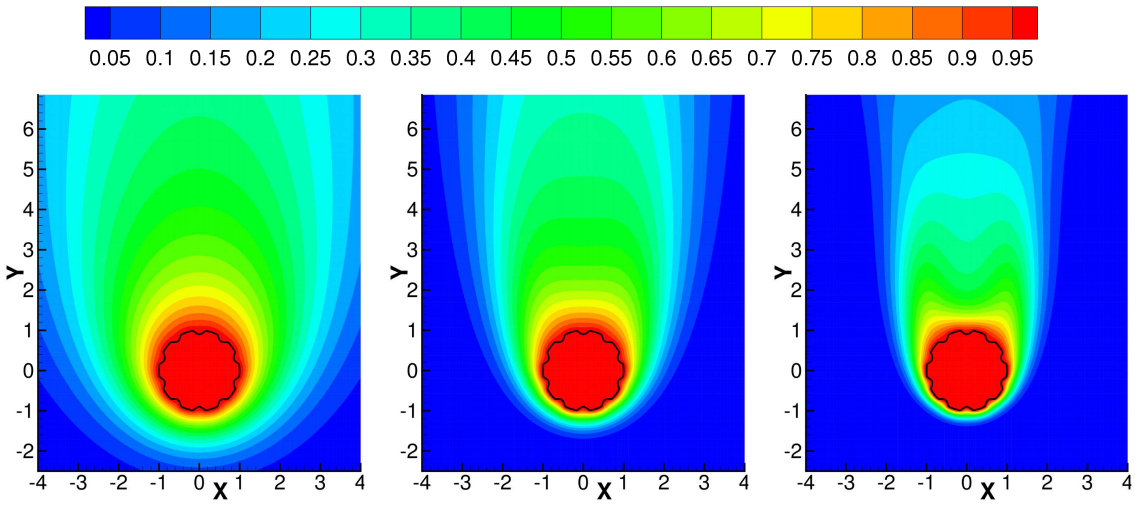

(a) Re = 10, $d = 0.1$, $S_{ef} = 1.08$ (b) Re = 40, $d = 0.1$, $S_{ef} = 1.08$ (c) Re = 100, $d = 0.1$, $S_{ef} = 1.08$

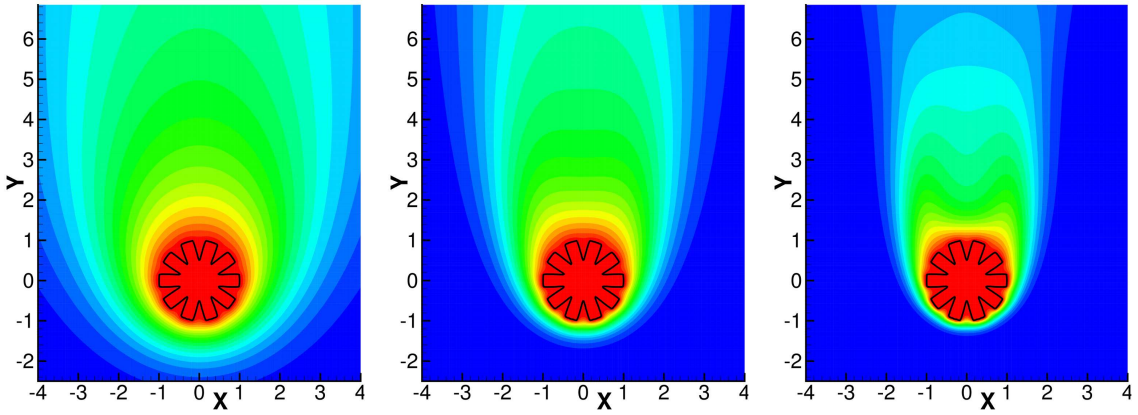

(d) Re = 10, $d = 0.5$, $S_{ef} = 2.12$ (e) Re = 40, $d = 0.5$, $S_{ef} = 2.12$ (f) Re = 100, $d = 0.5$, $S_{ef} = 2.12$

Figure 6: Contour plots of the isotherms $\frac{T-T_\infty}{T_s-T_\infty}$ for different Re and roughnesses.

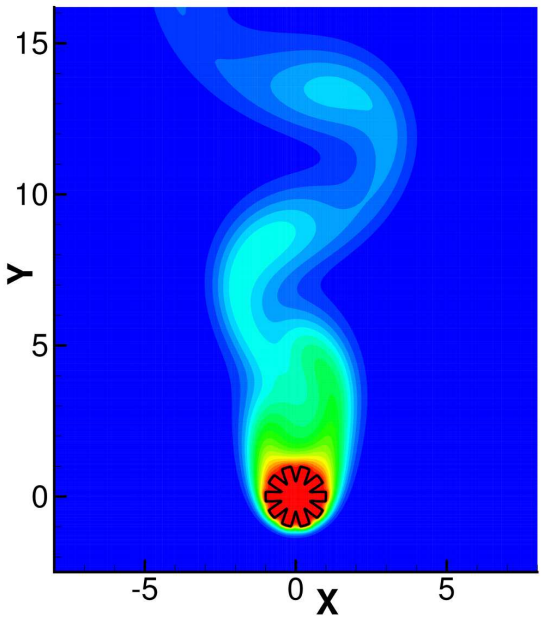

Figure 7: Snapshot of the isotherms $\frac{T-T_\infty}{T_s-T_\infty}$ for the $Re = 100$ and $S_{ef} = 2.12$.

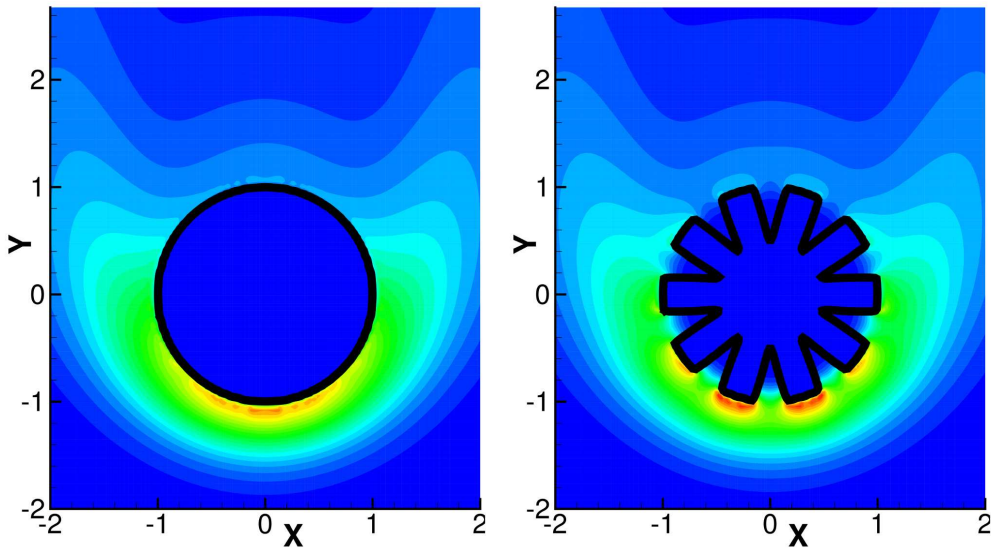

Figure 8: Contour plots of the non-dimension temperature gradient $\sqrt{\frac{\partial T}{\partial x}^2 + \frac{\partial T}{\partial y}^2}\frac{2R}{\Delta T}$ for $Re = 40$ and $S_{ef} = 1$ (left), and $S_{ef} = 2.12$ (right), respectively. The maximum in the left figure is 5.2 and the maximum in the right figure is 5.81.

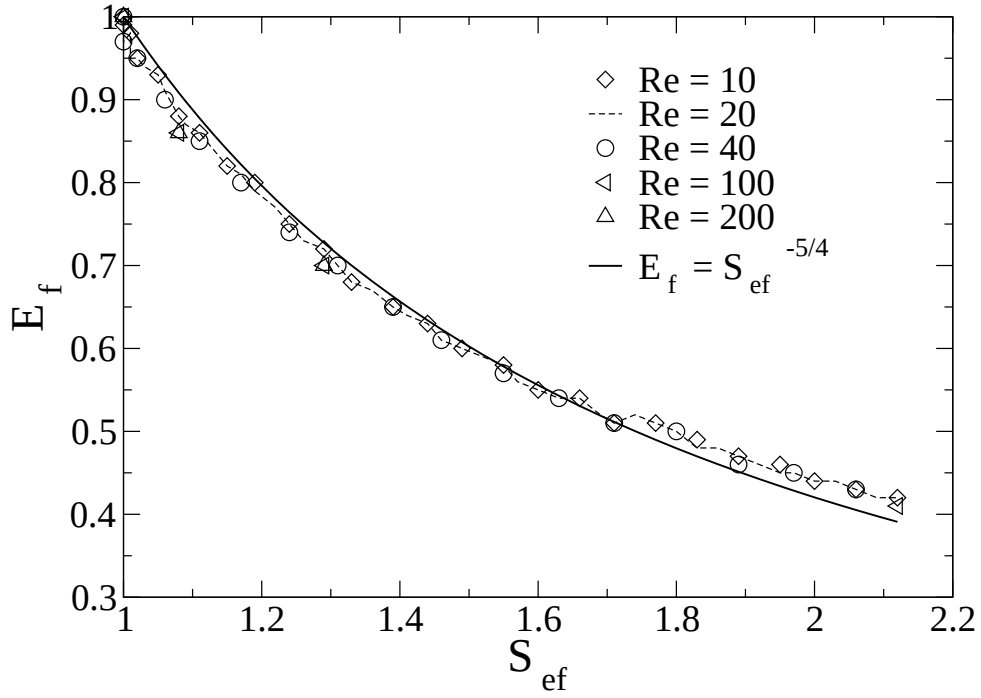

Figure 9: Effect of surface enlargement(S_{ef}) on the efficiency factor (E_f).

5 Conclusions

A numerical investigation of steady laminar and unsteady flow past a heated cylindrical particle with different roughness was carried out. The effect of the thickness of the roughness layer on the flow and heat transfer were systematically investigated. Based on the presented numerical data and discussions several conclusions can be summarized as follows:

1. The roughness has significant impact on the surface averaged Nusselt number. In particular, the Nusselt number decreases rapidly with increase of the roughness thickness.

2. The dependency of the efficiency factor E_f on the surface enlargement coefficient S_{ef} can be approximated by use of the following relation $E_f \approx S_{ef}^{-\frac{5}{4}}$ for $10 \leq Re \leq 200$.

3. The impact of the roughness on the drag coefficient is small in comparison to the surface averaged Nusselt number.

Acknowledge

This work was financially supported by the Government of Saxony and the Federal Ministry of Education and Science of Federal Republic of Germany as a part of CIC VIRTUHCON. The administration of TUBAF is gratefully acknowledged for the support. Authors thank Steffen Weise for his helpful comments and carefull reading of the manuscript. The Academic Communication and Computing Center of TU Bergakademie Freiberg is gratefuly acknowledged for the assistance in the use of HPC cluster.

REFERENCES

[1] H. Schlichting and K. Gersten, Grenzschicht-Theorie, *Springer*, **10th Edition** (2006).

[2] B. Fornberg, A numerical study of steady viscous flow past a circular cylinder, *J. Fluid Mech.*, **4**, 819–855 (1980).

[3] M. Braza, P. Chassaing and Ha. Minh, Numerical study and physical analysis of the pressure and velocity fields in thenear wake of a circular cilinder, *J. Fluid Mechanics*, **165**, 79-130 (1986).

[4] X. He and G. Doolen, Lattice Boltzmann Method on Curvilinear Coordinates System: Flow around a Circular Cylinder, *J. Comput. Phys.*, **134**, 306–315 (1997).

[5] Gh. Juncu, Unsteady conjugate heat/mass transfer from a circular cylinder in laminar crossflow at low Reynolds numbers, *Int. J. Heat Mass Transfer*, **47**, 2469–2480 (2004).

[6] S. Bhattacharyya and A.K. Singh, Augmentation of heat transfer from a solid cylinder wrapped with a porous layer, *Int. J. Heat Mass Transfer*, **52**, 1991–2001, (2009).

[7] I. E. Sutherland and G. W. Hodgman, Reentrant Polygon Clipping, *Communications of the ACM (CACM)*, **17**, 32–42, (1974).

[8] S.V. Patankar, Numerical Heat Transfer and Fluid Flow, *Hemisphere Publishing Corporation* (1980).

[9] J. Ferziger and M. Peric, Computational Methods for Fluid Dynamics, *Springer*, **3nd Edition** (2002).

[10] C.M. Rhie and W.L. Chow, Numerical study of the turbulent flow past an airfoil with trailing edge separation, *AIAA*, **21**, 1525–1532 (1983).

[11] T.H. Kuehn and R.J. Goldstein, An experimental and theoretical study of natural convection in the annulus between horizontal concentric cylinders, *J. Fluid Mech.*, **74**, 695–719 (1976).

[12] T.H. Kuehn and R.J. Goldstein, An experimental study of natural convection heat transfer in concentric and eccentric horizontal cylindrical annuli, *Journal of Heat Transfer*, **100**, 635–640 (1978).

[13] R. Mittal and G. Iaccarino, Immersed boundary methods, *Annu. Rev. Fluid Mech.*, **37**, 239–261 (2005).

[14] K. Khadra, P. Angot, S. Parneix and J.P. Caltagirone, Fictitious domain approach for numerical modelling of Navier-Stokes equations, *Int. J. Numer. Methods Fluids*, **34**, 651–684 (2000).